EPJ manuscript No.
(will be inserted by the editor)

Isotopic compositions and scalings

M.Colonna[1] and M.B.Tsang[2]

[1] Laboratori Nazionali del Sud INFN, via S.Sofia 62, I-95123 Catania, Italy and Dipartimento di Fisica e Astronomia, Universita' di Catania
[2] National Superconducting Cyclotron Laboratory and Department of Physics and Astronomy, Michigan State University, East Lansing, MI 48824, USA

Received: date / Revised version: date

Abstract. We review experimental and theoretical studies devoted to extract information on the behaviour of the symmetry energy, in density regions different from the normal value, from charge - asymmetric reactions at Fermi energies. In particular, here we focus on the analysis of fragmentation reactions and of isotopic features of fragments and light charged particles. Results concerning "isoscaling" properties and the N/Z equilibration among the reaction partners in semi-peripheral reactions are also analyzed.

PACS. 21.30.Fe - 25.70.-z - 25.70.Lm - 25.70.Pq

1 Introduction

Heavy ion collisions at Fermi energies offer the possibility to learn about properties of the nuclear effective interaction in regions where the density and temperature are different from those for stable nuclei. In particular, in charge asymmetric systems, one can access information on the behaviour of the symmetry energy, E_{sym}, that is poorly known at low and high densities. Not only is the symmetry energy relevant for structure properties, being clearly linked to the thickness of the neutron skin in heavy nuclei (see [1]),but this information is of interest also in the astrophysical context, providing constraint to the effective interactions used in astrosphysical calculations [2,3]. Such information is indeed essential for the understanding of the properties of supernovae and neutron stars [4–9].

In Fig.1 (bottom panel) we show the density dependence of the potential symmetry energy contribution, $E_{sym,pot}$ for three different effective interactions. While all curves cross at normal density ρ_0, large differences are present for values, slopes and curvatures, particularly in high density regions. Even at the relatively well known "crossing point" at normal density the various effective forces are presenting controversial predictions for the momentum dependence of the fields acting on the nucleons and, consequently, for the splitting of the neutron/proton effective masses, which are important in nuclear structure and nuclear reaction dynamics. For discussion purpose, we will call interaction such as BPAL32 as "stiff", or "soft" for SKM* (Fig.1).

Fragmentation mechanisms at Fermi energies can be used to study the symmetry energy at densities below and around the normal value. In violent collisions, where the full disassembly of the system into many fragments is observed, one can study new properties of liquid-gas phase transitions occurring in asymmetric matter. In neutron-rich matter, phase co-existence leads to a different asymmetry in the liquid and gaseous phase: fragments (liquid) appear more symmetric with respect to the initial matter, while light particles (gas) are more neutron-rich [10–14]. This effect, that is simply related to the fact that the

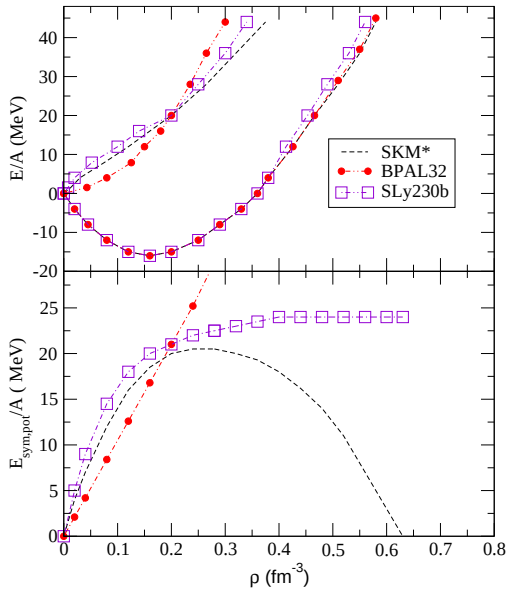

Fig. 1. Equation of State (EOS) for various effective forces. Top: neutron matter (up), symmetric matter (down). Bottom: potential symmetry energy.

Send offprint requests to:

symmetry energy decreases when the density gets lower, can be used to investigate the behaviour of the derivative of the symmetry energy with respect to density. Hence fragmentation studies allow one to get information on the low-density properties of the symmetry energy. Complementary information is obtained from the study of emitted nucleons and light particles (pre - equilibrium phase).

Moreover, the importance of the isotopic degree of freedom to obtain information about charge equilibration and its relation to the charge asymmetry dependent terms of the EOS has been recently pointed out [15]. The mechanisms responsible for isospin transport can be essentially related to the presence of isospin, but also density gradients along the reaction path. Isospin diffusion bears information about the value of the symmetry energy at low density, while the drift (transport in the presence of density gradients) is more connected to the derivative of the symmetry energy.

Isospin effects on observables of interest in intermediate energy heavy ion collisions have been studied by using isospin-dependent quantum molecular dynamics models (IQMD) [16,17], the anti-symmetrized molecular dynamics (AMD) model [18] and (stochastic) mean-field models (BUU,BNV,SMF) [19–21]. We will review here experimental and theoretical results about isotopic properties of reaction products, with the aim of extracting the available information about the behaviour of the symmetry energy. The paper is organized as it follows: We will first review results concerning the isotopic content and properties of pre - equilibrium emission, then we will discuss fragment production and the relation of fragment isotopic distributions to the symmetry energy behaviour, focusing in particular on the recently introduced isoscaling analysis. Finally we will discuss isospin transport mechanisms in mid-peripheral reactions and N/Z equilibration, before concluding.

2 Isospin effects on pre-equilibrium emission

Heavy ion reactions, at energies larger than 30-40 MeV/A, are characterized by fast particle emissions, that happen before and during the path of the system towards thermalization. This particle production is often referred to as pre-equilibrium emission, see Ref.[22] and references therein.

For nuclear collisions around the Fermi energies, fast particle emission happens mostly during the expansion phase, when the composite system has reached density values below the normal one. Hence this study allows one to extract information on the behaviour of the symmetry energy at sub-normal densities. In collisions between neutron-rich nuclei, the N/Z of the pre-equilibrium emission will directly reflect the value of the symmetry energy (being larger for larger values of E_{sym}). In dynamical models as in BNV (or BUU) models, as well as in stochastic mean-field simulations, we observe a different N/Z composition of pre-equilibrium emission depending on the asy-EOS. At low density, the symmetry energy is larger in the "soft" case favoring neutron emission. These results and interpretation are confirmed also by molecular dynamics studies, as discussed below.

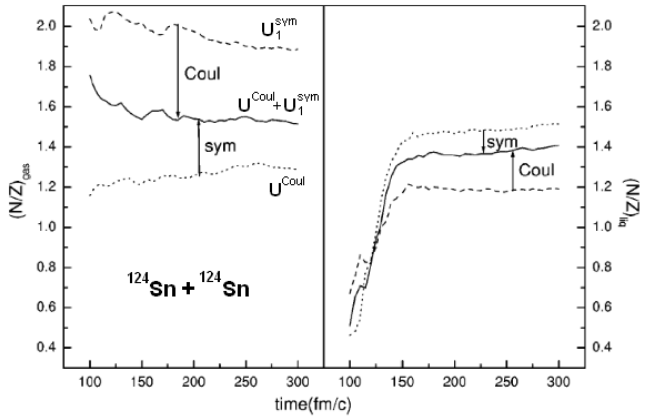

Fig. 2. The time evolution of $(N/Z)_{gas}$ (left window) and $(N/Z)_{liq}$ (right window) for three combinations of Coulomb and symmetry interactions, for the reaction ^{124}Sn + ^{124}Sn at 50 MeV/A and impact parameter b=2 fm, as obtained in IQMD.

We will define as emitted particles (the "gas phase") those particles localized in low-density regions ($\rho < \rho_0/3$ for instance), while the remaining matter will be identified as "liquid phase". Pre-equilibrium emission can be associated with particles emitted (gas phase) at the first collisional stage, i.e. up to $\approx 100 fm/c$. Obviously the properties of the "liquid phase" will also be influenced by the characteristics of this particle emission. Fig.2 shows the time evolution of $(N/Z)_{gas}$ and $(N/Z)_{liquid}$, for the reaction ^{124}Sn +^{124}Sn at 50 MeV/A, b= 2 fm, obtained with the IQMD model considering the full nucleon-nucleon interaction (full line), or suppressing Coulomb (dashed line) or symmetry potential (dotted line). A "stiff" parameterization has been used for the symmetry energy. It is clear that the Coulomb interaction reduces the N/Z of the pre-equilibrium emission, while the symmetry energy enhances it. At $t \approx 150 fm/c$ one obtains $(N/Z)_{gas} \approx 1.5$ while $(N/Z)_{liquid} \approx 1.4$. Hence the gas phase is more neutron-rich.

It is worthwhile comparing quantitatively the results obtained with the different transport models. In ref.[32], the same reaction has been studied with the BUU code. For the "stiff" parameterization, for the N/Z of the liquid phase, values around 1.44 are obtained at t=100 fm/c (a "soft" parameterization leads to $N/Z = 1.23$). The value compares rather well (within 3%) with the results of the IQMD model. The different time scales in the two models depend on the definition of "liquid phase", that for IQMD corresponds to cluster and intermediate mass fragment (IMF) emission, while in the BUU model it is associated with a composite excited source. As shown in Fig.3 these results are also in agreement with stochastic mean field (SMF) simulations. Indeed, we observe that, with a "stiff" parameterization of the symmetry energy, after around 100 fm/c, the asymmetry of the liquid phase equals 0.18, that corresponds to $N/Z = 1.44$.

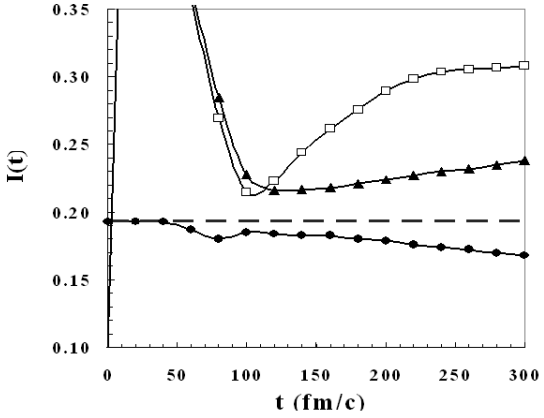

Fig. 3. Time evolution of the asymmetry of the liquid phase (circles), gas phase (triangles) and gas phase in a central region (squares), for the reaction $^{124}Sn + ^{124}Sn$ at 50 MeV/A, b= 2 fm, SMF calculations. A "stiff" parameterization of the symmetry energy has been used.

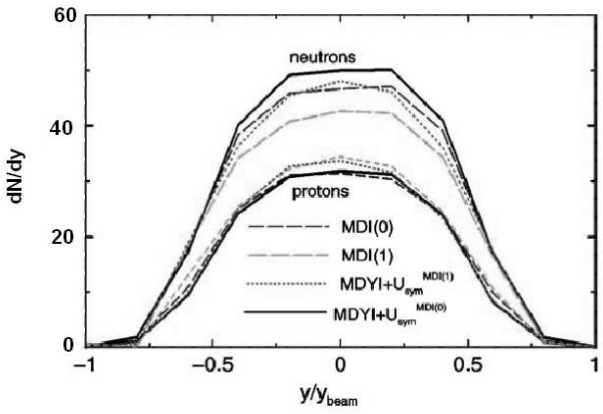

Fig. 4. Rapidity distributions of neutrons and protons, obtained in the reaction $^{132}Sn + ^{124}Sn$ at 400 MeV/A, b = 5 fm. The results of four interactions are presented: the MDI(0), "stiff" (thick dashed line) and MDI(1), "soft" (grey dashed line), that contain momentum dependence also in the isovector part of the interaction; the MDYI(0) (thick solid line) and MDYI(1) (dotted line), that are without iso-momentum dependence.

AMD simulations for different Ca isotopes at 35 MeV/A are studied in ref.[18]. For the $^{48}Ca + ^{48}Ca$ reaction, that has roughly the same asymmetry of $^{124}Sn + ^{124}Sn$ reaction, one observes that after $\approx 80fm/c$, $(Z/A)_{liq} = 0.42$ corresponding to $N/Z = 1.39$ (using "stiff" equation of state, Gogny-AS). However, at later times, $t \approx 300fm/c$, the liquid phase appears more symmetric in the BUU calculations [18]. This indicates that the rate of neutron enrichment of the gas phase is not the same in the two models. This may be related to the different evolution of the system in the two models. Indeed AMD calculations can describe the disassembly of the excited system into many clusters, while in BUU calculations only a composite single excited source, that emits nucleons, not clusters, survives until late times. The isospin content of fragments formed in dissipative collisions at intermediate energies will be discussed in next section.

It is interesting to look at the behaviour of pre - equilibrium emission in reactions at higher beam energies [23–25]. Indeed in this case particles are emitted mostly from the high density (compression) phase, hence one tests the behaviour of the symmetry energy at densities above saturation. Pre-equilibrium emission is also sensitive to the momentum-dependent part of the iso-vector interaction. Typical BUU calculations are shown in Fig.4, for the reaction $^{132}Sn + ^{124}Sn$ at 400 MeV/A. The results obtained with four interactions are presented: two without momentum dependence in the iso-vector part of the nuclear interaction (MDYI) and two momentum dependent interactions (MDI), with a different density behaviour of the symmetry energy, "soft" (1) or "stiff" (0). The figure shows rapidity distribution of pre-equilibrium neutrons and protons, at b=5 fm. One can see that, with an asy-"stiff" parameterization, more neutrons are emitted. Indeed the symmetry energy is higher in the high density phase. Moreover, it is possible to observe that less neutrons are emitted in the case where the momentum dependence is implemented (compare the thick full and dashed lines for instance). Indeed, for the interactions considered here, one obtains a splitting of neutron and proton effective masses with $m^*_n > m^*_p$ and this reduces the neutron repulsion. Therefore we observe a kind of compensation between the effects due to the density dependence and to the momentum dependence of the symmetry potential. In fact, the thick dashed line ("stiff" interaction with momentum dependence) and the dotted line ("soft" interaction without momentum dependence) almost overlap. On the other hand, considering interactions with the opposite splitting, $m^*_n < m^*_p$, neutrons would be more repulsed [24,26]. In Fig.5 the neutron to proton ratio is plotted as a function of transverse momentum, for particles in the mid-rapidity region. From the figure it is clear that the decrease of N/Z observed with the MDI interactions (see Fig.4) can be attributed to the high momentum tail of the nucleon emission that is more sensitive to the momentum dependence.

In summary, the study of pre-equilibrium emission, as a function of the beam energy, can be considered as an interesting and promising tool to explore the reaction dynamics and to investigate the behaviour of the symmetry energy from low to high density. The isotopic or neutron-proton composition, N/Z, of all emitted particles appears to be sensitive to the stiffness of the symmetry energy while the dependence of the isotopic content on rapidity, or transverse momentum, appears as a good candidate to learn about the momentum dependence of the isovector part of the nuclear interaction.

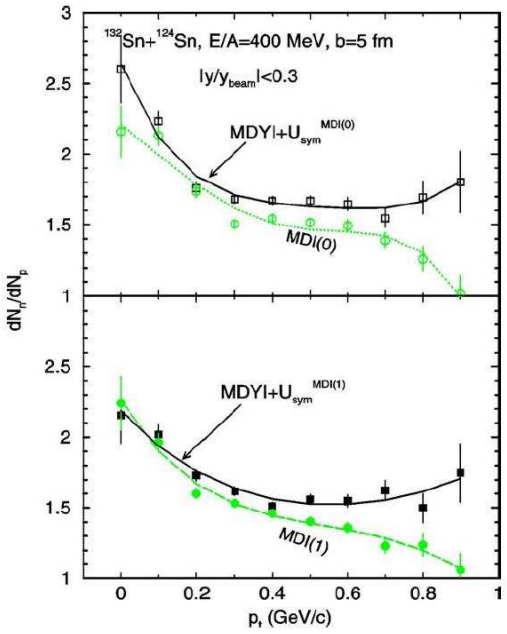

Fig. 5. Neutron to proton ratio, as a function of transverse momentum, for the same reaction and interactions of Fig.4.

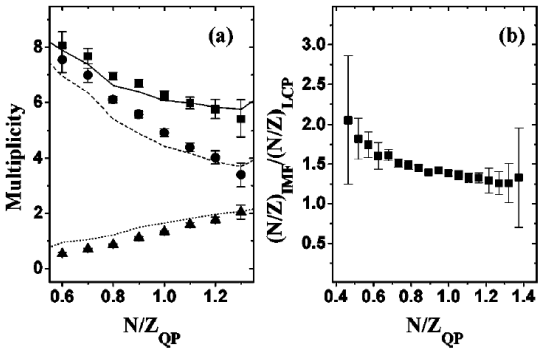

Fig. 6. a) Multiplicity of all charged particles (squares) as a function of the N/Z of the emitting PLF source, obtained in the reaction $^{28}Si + ^{112}Sn$ at 50 MeV/A. Circles and triangles represent the multiplicity of LCP's and IMF's, respectively. The lines are the results of model calculations. b)The ratio between the N/Z of IMF's and LCP's is plotted as a function of the N/Z of the PLF source.

3 Isotopic composition of fragments: the iso-distillation

Observables connected to the study presented in the previous section are the isotopic properties of the IMF's formed in dissipative collisions at intermediate energies, that can be investigated with (statistical or dynamical) multifragmentation models, by following the reaction until late times. The isotopic composition of nuclear reaction products provides important information on the reaction dynamics and the possible occurrence of a phase transition in asymmetric nuclear matter [10,11,27], which is supposed to lead to separation into a symmetric dense phase (fragments) and asymmetric dilute phase (nucleons and light particles) [27,28,11]. Such a phase transition can be generated by fluctuations of density or concentration, leading to a coupling of different instability modes. This mechanism is predicted, for instance, by stochastic mean-field (SMF) simulations [21], where fragment formation happens due to the development of spinodal (volume) instabilities.

After the initial collisional shock, or due to thermal expansion effects, the excited nuclear system expands and enters the low density (co - existence) region of the nuclear matter phase diagram. Here a phase separation occurs and fragments are formed, surrounded by a neutron-rich gas phase. This process is often referred to as isospin distillation or fractionation [13,28]. As one can see from Fig.3,after the first stage of particle emission, the asymmetry of the liquid phase still decreases while fragments are formed. This is because fragmentation is accompanied by the iso-distillation process. The amplitude of the effect is strictly related to the behaviour of the symmetry energy, as we will discuss more in detail in the section devoted to isospin transport. Hence an experimental analysis of the N/Z of reaction products provides precious complementary information about the low-density dependence of the symmetry energy.

3.1 Experimental evidence

The N/Z degree of freedom has been studied experimentally in detailed measurements of isotopic distributions of the emitted fragments [29,30,15]. Isotopically resolved data in the region $Z = 2 - 8$ have revealed systematic trends, which however are substantially affected by the decay of primary fragments. As we will see in the following discussion, the effect of sequential decay of primary fragments may be reduced, in some cases, by comparing the yields of fragments from two similar reactions.

The composition of intermediate mass fragments in several conditions of isospin asymmetry and excitation energy of the fragmenting source has been studied, for instance, by considering quasi - projectiles created via peripheral reactions of $^{28}Si + ^{112}Sn$ and ^{124}Sn at 30 and 50 MeV/A [31]. The quasi - projectiles have been reconstructed from completely isotopically identified fragments. The difference in N/Z of the reconstructed quasiprojectiles allows the investigation of the disassembly as a function of the isospin of the fragmenting system. It is observed that the dependences of mean fragment multiplicity and mean N/Z ratio of the fragments on N/Z ratio of quasi-projectiles are different for light charged particles (LCP) and intermediate mass fragments. This is illustrated in Fig.6, for the reaction $^{28}Si + ^{112}Sn$ at 50 MeV/A. The squares represent the multiplicity of all charged particles. This is then broken down into the multiplicity of light charged particles (circles) and the multiplicity of intermediate mass fragments (triangles). We can see that the IMF multiplicity increases with the N/Z of the system. The lines represent the results of hybrid calculations, obtained by combining a description of transfer processes in

Deep-inelastic reactions (DIT model) to statistical calculations of fragment production (Statistical Multifragmentation Model, SMM). They are in good agreement with the data. As shown also in [32,29], the multiplicity of IMF's as a function of multiplicity of charged particles increases for the more neutron-rich systems. However, the decrease in multiplicity of LCP's for neutron-rich systems in Fig.6 is not observed in the multifragmentation of Sn+Sn system [33].

This effect, however, weakens at higher energies [34]. This is consistent with the temperature dependence of the isospin distillation effect extracted from the lattice-gas model [35] or from dynamical calculations [21]. The ratio $(N/Z)_{IMF}/(N/Z)_{LCP}$ decreases with increasing N/Z_{QP}, as shown in Fig.6(b). As there are fewer neutrons available, the excess protons go into the smaller fragments rather than the larger ones. Neutron-poor quasi-projectiles prefer to break up into very neutron-deficient (proton rich) LCP's and much more symmetric IMF's. On the contrary, neutron-rich quasi-projectiles breaks up into neutron-rich LCP's and more symmetric IMF's, the distillation effect discussed before [13,28].

A comparison between experimental isotopic distributions, obtained for IMF's in the Sn + Sn systems [33], and theoretical predictions (SMF simulations) indicates a better agreement when a "stiff" asy-EOS is used [36].

The fact that the number of produced IMF's is larger in neutron-rich systems is nicely confirmed by recent ALADIN data, where the disassembly of excited quasi - projectiles is studied [37]. More IMF's are produced in the neutron rich system, ^{124}Sn, with respect to ^{107}Sn. In fact in the neutron-rich case protons go mostly into IMF's, while in the proton-rich case they are concentrated into LCP's (see also the previous results [31]).

As for the evolution of the N/Z of fragments with the excitation energy of the fragmenting source, this is found to increase, as shown in Ref.[38] for fragments emitted from excited PLF sources (see Fig.7). From the statistical point of view, this can be explained in terms of the larger amount of excitation energy available, that allows production of more exotic systems in a larger phase space. This effect is also compatible with the weakening of the distillation mechanism at high temperature, as discussed above.

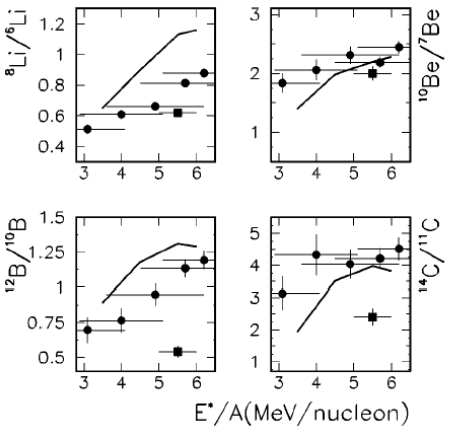

Fig. 7. Ratios of relative yields of neutron-rich to neutron-deficient isotopes, as a function of the excitation energy, as obtained in the fragmentation of PLF sources, from Au + Au, 35 AMeV (circles) or in central Xe + Cu (30 AMeV) collisions (squares). The lines are the predictions of SMM calculations.

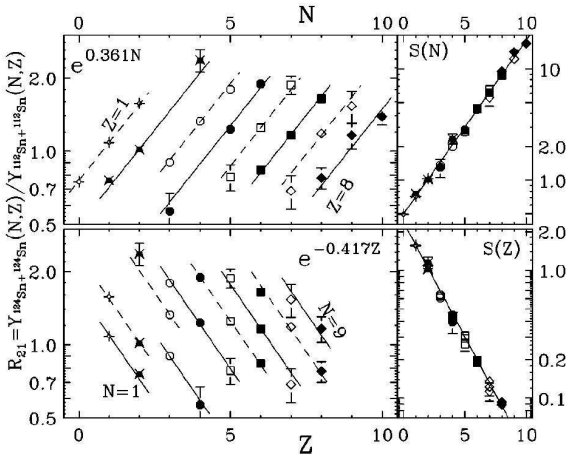

Fig. 8. The yield ratio R_{21} is plotted as a function of N (upper panel) or Z (lower panel). The central reactions considered are $^{124}Sn+^{124}Sn$ and $^{112}Sn+^{112}Sn$, at 50 MeV/A.

4 Isoscaling in nuclear reactions

The availability of fragmentation data, with good isotopic resolution, obtained with charge - asymmetric systems, makes it possible to examine systematic trends exhibited by isospin dependent observables. In a series of recent papers, the scaling properties of cross sections for fragment production with respect to the isotopic composition of the emitting systems were investigated in [29,30]. The studied reactions include symmetric heavy ion reactions at intermediate energy, leading to multifragment emission, as well as asymmetric reactions induced by α particles and ^{16}O projectiles at low to intermediate energies with fragment emission from excited heavy residues. To quantify the comparison of the isotope yields $Y(N,Z)$ obtained in reactions with different isospin asymmetry, the ratio $R_{21} = Y_2(N,Z)/Y_1(N,Z)$ is used. By convention, 2 denotes the more neutron-rich system. Fig.8 shows the isotope ratios, $R_{21}(N,Z)$, plotted as a function of N (upper panel) and Z (lower panel), for the central collisions of $^{124}Sn+^{124}Sn$ and $^{112}Sn+^{112}Sn$, at 50 MeV/A. $R_{21}(N,Z)$ clearly exhibits an exponential dependence on N and Z, which is called the isoscaling relationship:

$$R_{21}(N,Z) = Y_2(N,Z)/Y_1(N,Z) = C \cdot exp(N \cdot \alpha + Z \cdot \beta), \quad (1)$$

where C, α and β are the fitting parameters. Since the introduction of isoscaling as an isospin observable, it has proved to be very robust and has been observed in many different types of reactions, such as multifragmentation, light ion induced fragmentation, evaporation and deep-inelastic reactions [29,30,39,40]. There are also reports

on the observation of isoscaling in spallation reactions [41] and, more recently, in fission [42], though the quality of the data is quite poor. Recent studies with realistic fission models [43] suggest that the behaviour of the isoscaling observed in fission is not the same as those observed in multifragmentation, e.g. the neutron isoscaling parameter, α, varies with Z of the fission products. However, as with the other reactions, the isoscaling observed in fission appears connected to the symmetry energy and the temperature of the system, as we will see below.

4.1 Isoscaling in statistical models

In the grand canonical statistical description of multifragmentation, the mean multiplicity of a fragment with mass number A and charge Z is given by:

$$< N(A,Z) >= g_{AZ}\frac{V_f}{\lambda_T^3}A^{3/2}exp[-\frac{1}{T}(F_{AZ}(T,\rho) - \mu_n(A-Z) - \mu_p Z)], \quad (2)$$

where T is the temperature of the fragmenting source, g_{AZ} is the degeneracy factor of the fragment, λ_T is the nucleon thermal wavelength, V_f is the "free" volume, F_{AZ} is the fragment free energy and μ_n and μ_p are the neutron and proton chemical potentials, respectively. It follows immediately that, for two systems 1 and 2 with different total mass and charge but with the same temperature and density, the ratio of fragment yields is given by Eq.(1) with parameters $\alpha = \Delta\mu_n/T$ and $\beta = \Delta\mu_p/T$. Isoscaling arises very naturally within a statistical description of fragment production. Within such a scheme, it is the difference of the chemical potentials of systems with different N/Z ratio that is directly connected with the isoscaling phenomenon.

In ref.[44], the chemical potentials for ^{124}Sn and ^{112}Sn are calculated with the grand-canonical version of the statistical multifragmentation model. Despite a considerable variation of the individual potentials, their difference $\Delta\mu = \mu_{112} - \mu_{124}$ changes only slightly as a function of the temperature. The results are similar to that obtained with the Markov chain version of the Statistical Multifragmentation Model (SMM), which takes a completely microcanonical approach, at temperatures $T > 5\ MeV$, which are of relevance for the production of fragments. At low temperature results diverge indicating that the exact conservation of charge, mass and energy really makes important differences with respect to the grand-canonical approximation. Calculating the difference of chemical potentials within the grand-canonical approximation, it is possible to connect the isoscaling parameter α to the difference of asymmetry between the two systems considered and the value of symmetry energy and temperature, through the relation:

$$\xi = \alpha/(4\Delta(Z/A)^2) = E_{sym}/T \quad (3)$$

An analogous relation is derived for β. Isoscaling is not limited to models within the grand canonical approximation. As matter of fact, this equation was first derived in the expanding emitting source EES model [45,46]. Rather, isoscaling predictions have been observed from different statistical multifragmentation models: canonical and micro-canonical models [46,47],and lattice-gas calculations [48].

There is a simple explanation within the SMM why isoscaling should appear in finite systems. In most SMM models, a mass formula, usually a variant of the liquid-drop mass formula, is used. Charge distribution of fragments with fixed mass numbers A, as well as mass distributions for fixed Z, are approximately Gaussian with average values and variances which are also connected with the temperature and the symmetry energy coefficient [44]. With a Gaussian distribution for the charge Z, for instance, we obtain, for fragments with a given mass A: $Y(Z) = exp(-(Z- < Z >)^2/2\sigma_Z^2)$. The ratio of this observable for two different systems is given by:

$$Y_2(Z)/Y_1(Z) = c\ exp(-Z^2/2(1/\sigma_2^2 - 1/\sigma_1^2) + Z(< Z >_2/\sigma_2^2 - < Z >_1/\sigma_1^2)) \quad (4)$$

If the variances σ_1 and σ_2 are equal, then isoscaling is observed. Also, since the variance σ_Z is approximately equal to $\sigma_Z \approx \sqrt{(}AT/8E_{sym})$, it turns out that the same expression for β, as in the grand-canonics, is obtained.

In cases when the experimental masses are used, the isotope distributions are not strictly Gaussian. Fig.9 shows the hot carbon isotope distributions predicted by the canonical SMM model (open circles, top panel) from a source with A=186, Z=75 and T=5 MeV, $\rho/\rho_0 = 1/6$.

The solid circles correspond to the isotope distributions after sequential decays. Neither the primary nor the final distributions are Gaussian. Nonetheless, from two fragmenting sources with different N/Z, one can derive the yield ratios (and observe isoscaling), that are plotted in Fig.10 for primary and final fragments. As one can see from the Figure, isoscaling parameters are only slightly modified by the secondary decay process, as far as the standard value of the symmetry energy coefficient is used in the SMM. However, the effect of secondary decay depends on the symmetry energy value employed [49] and is much larger with dynamical models, where chemical equilibrium is not necessarily reached.

4.2 Origin of Isoscaling in reaction dynamics

Isoscaling has been observed also in dynamical fragmentation models, such as the Antisymmetrized Molecular Dynamics (AMD) model [18] , Quantum Molecular Dynamics (QMD) and Classical Molecular Dynamics (CMD) [50], as well as in Stochastic Mean Field (SMF) calculations [36] and in quasi-analytical calculations of the spinodal decomposition process [51]. For instance, Figure 11 shows the dependence of α on the charge to mass ratio, $(Z/A)^2$, of the liquid phase for the collisions of Ca isotopes, at 35 MeV/A, as predicted by the AMD model. A linear dependence of α on $(Z/A)^2$ is observed. The two lines correspond to two different symmetry potentials used in the simulations (full line-"soft"-Gogny; dashed

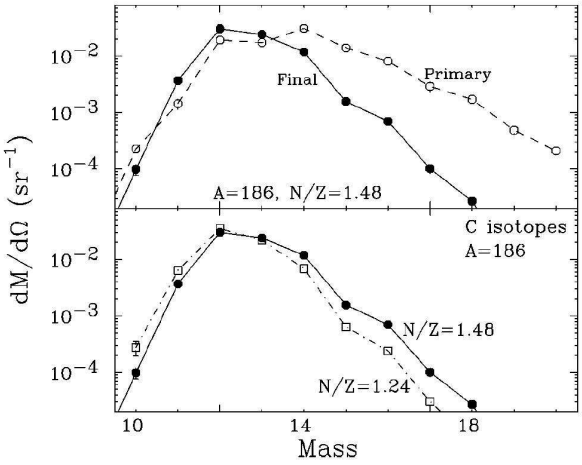

Fig. 9. Top: Mass distribution of Carbon isotopes, as obtained for the indicated systems, in SMM calculations, for primary hot fragments and final fragments. Bottom: Predictions for final fragments are compared for two systems with different N/Z.

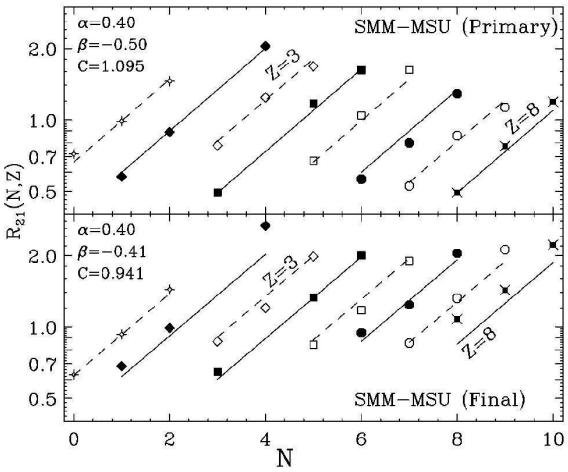

Fig. 10. The isotope yield ratio, as obtained for the systems of Fig.9, is plotted as a function of N for primary (top) and final (bottom) fragments.

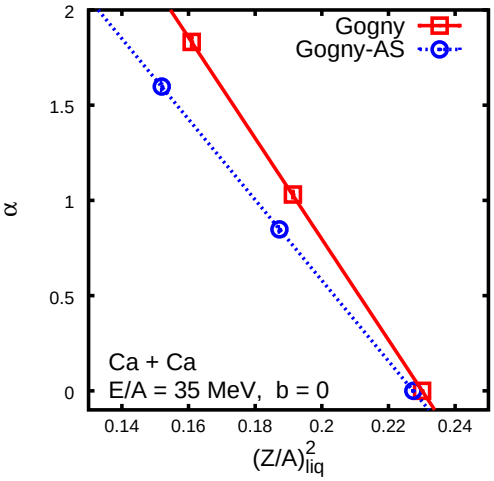

Fig. 11. Isoscaling parameter α, as a function of $(Z/A)^2_{liq}$ between the two compared systems, as obtained in AMD calculations with two different parameterizations of the symmetry energy.

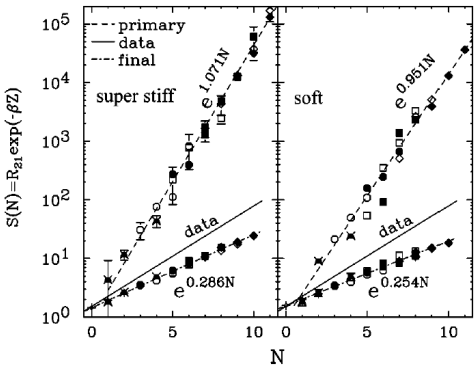

Fig. 12. Scaled isotope yield ratio, as a function of N, as obtained in SMF calculations of central reactions $^{124}Sn+^{124}Sn$ and $^{112}Sn+^{112}Sn$, at 50 MeV/A, for primary and final fragments. Two parameterizations of the symmetry energy are considered.

line-"stiff"-GognyAS). Thus, even in dynamical models, isoscaling is intimately related to the symmetry energy. However, unlike statistical models, secondary decays have much larger effects on the primary fragments. Thus in general, secondary decays reduce the differences in isoscaling arising from different symmetry terms in the EOS used in the models [52].

For example, the results of SMF, based on the spinodal decomposition scenario, are presented in Fig.12 [36]. Here large isoscaling parameters are observed for the primary fragments. However, they are significantly affected by the secondary decay and final values appear closer to the data. But the relative differences between the two parameterizations of the symmetry energy used are also much reduced.

The study of isoscaling through dynamical simulations can elucidate the origin of this phenomenon. If chemical equilibrium is reached during the fragmentation process, it is clear that one can apply the considerations outlined in the previous section and directly relate the isoscaling parameter to the value of the symmetry energy and the temperature.

However, the linear relation between α and $(Z/A)^2$ can be obtained also in different conditions, without assuming statistical equilibrium. If the origin of fluctuations in a multi-fragmenting systems can be considered a "white noise" source, then the probability to observe a given fluctuation of the isovector density $\delta\rho_i = \delta\rho_n - \delta\rho_p$, in a given volume V, can be expressed (for small amplitude fluctuations) as:

$$P \approx exp(-\delta\rho_i^2/2\sigma_{\rho_i}), \qquad (5)$$

where the variance σ_{ρ_i} depends on the fragmentation mechanism. Then, for a fragment of volume V and mass A, the distribution $P(N-Z)$ can be written as:

$$P(N-Z) \approx exp(-[N-Z-(\bar{N}-\bar{Z})]^2/(\mathcal{F}\rho_{in}V)), \quad (6)$$

where $\bar{N}$ and $\bar{Z}$ are the average neutron and proton numbers in the volume V, and σ_{ρ_i} is proportional to ρ_{in}, the density of the fragmenting system [53]. $\mathcal{F}$ is a constant that depends on the symmetry energy and the temperature.

In spinodal decomposition, for instance, fragments are formed (and their density grows) due to the development of isoscalar-like unstable modes. Hence isoscalar density fluctuations grow while the isovector variance does not evolve and keeps the memory of the initial isovector fluctuations of the unstable diluted source. Therefore we may expect reduced iso-vector fluctuations (and larger isoscaling parameters) with respect to the statistical case, where the isotopic content of the entire fragment mass may fluctuate. This is in line with the results of Fig.12.

The results obtained in a quasi-analytical description of spinodal decomposition, comparing fragment production in nuclear matter with asymmetry $I = 0.2$ and $I = 0.1$, are presented in Fig.13, for two parameterizations of the symmetry term [51].

The formula can be recast as follows

$$P(N-Z) \approx exp(-[(N-Z)^2/A - N(4(\bar{Z}/A)^2-1) - Z(4(\bar{N}/A)^2-1)]/[\mathcal{F}/\eta]) \quad (7)$$

where η is the ratio between the fragment final density $\rho_{fin} = A/V$ and the initial density ρ_{in} (η larger or equal to 1).

In statistical models η is equal to 1 and $\mathcal{F}$ coincides with T/E_{sym}, while in the spinodal decomposition process the variance of the fragment isotopic distribution, due to isovector fluctuations, is reduced with respect to the equilibrium value $\mathcal{F}$. However it should be noticed that, within such a scenario, also isoscalar-like modes contribute to the variance, due to the beating of several unstable modes, that bear a different distillation effect [51].

If one assumes that $\bar{Z}/A$ (and $\bar{N}/A$) depends only slightly on A and can be related to the average distillation effect, that determines the average asymmetry of the formed fragments, then from Eq.(7) one gets isoscaling. It is interesting to notice that the isoscaling parameters result equal to:

$$\alpha = 4((Z_1/A_1)^2 - (Z_2/A_2)^2)/(\mathcal{F}/\eta)$$
$$\beta = 4((N_1/A_1)^2 - (N_2/A_2)^2)/(\mathcal{F}/\eta). \quad (8)$$

Hence one gets the same formal expression as in statistical models, but with a more complex relation of the isoscaling parameters to the system properties. These parameters appear connected to the distillation effect, but also to the width of the isotopic distributions, that can in general differ from the predictions of statistical models.

In summary, the link between the isoscaling parameters and the symmetry energy depends on the way fragments are formed, while the observation of isoscaling and the relation to the (Z/A) value of the liquid phase appear as quite general properties and do not require the assumption of statistical equilibrium.

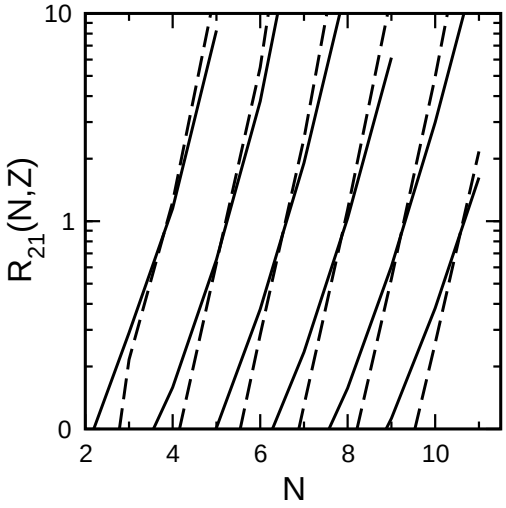

Fig. 13. Isotopic ratio $R_{21}(N,Z) = Y_{\alpha=0.2}(N,Z)/Y_{\alpha=0.1}(N,Z)$ calculated with the "superstiff" symmetry term (solid lines) and with the "soft" symmetry term (dashed lines). Lines correspond to different values of Z, $Z = 3-8$ from left to right. The system is prepared with density and temperature inside the spinodal region. The average values of the slope approximatively are 2.2 and 1.5 for the "soft" case and the super-"stiff" case respectively.

4.3 Temperature dependence of isoscaling

With the availability of models, we are able to explore the temperature dependence of isoscaling. All calculations (statistical or dynamical) agree on the fact that the isoscaling parameters are inversely related to the temperature. So we would expect these parameters to decrease with increasing temperature, excitation energy or incident energy. Indeed, such phenomenon was observed in Ref.[39, 54]. Figure 14 shows the isoscaling parameter α as a function of the incident energy. In this study, isobars with mass = 58 (namely ^{58}Ni and ^{58}Fe) are used as target and projectile. Reaction 1 is taken to be the symmetric $^{58}Ni + ^{58}Ni$ which has the initial N/Z value of 1.07. For the upper curve (solid points), reaction 2 is taken to be the symmetric system $^{58}Fe + ^{58}Fe$ with $N/Z = 1.23$ and, for the lower curve, the mixed system, $^{58}Fe + ^{58}Ni$, with initial $N/Z = 1.15$ is used as reaction 2. This figure clearly shows that the α value decreases with incident energy from E/A = 30 MeV to 47 MeV. In addition, there is also a clear drop in the α values with the decrease of the initial N/Z values of the entrance channel. The latter has also been observed in the collisions of central Sn isotopes which first established the phenomenon of isoscaling [29].

Isoscaling has been studied also in fragmentation processes of excited target residues, in the reactions $^{12}C + ^{112,124}Sn$ at 300, 600 MeV/A [49]. The isoscaling parameter α

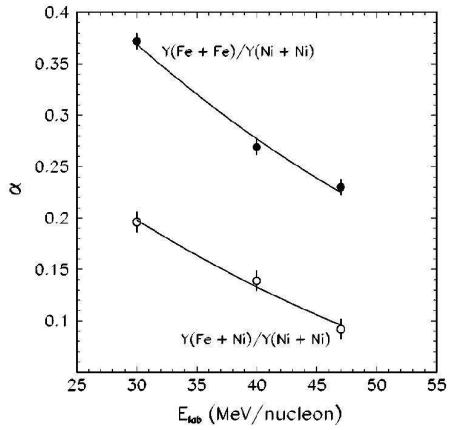

Fig. 14. Evolution of the isoscaling parameter α, as obtained in central collisions, versus the beam energy.

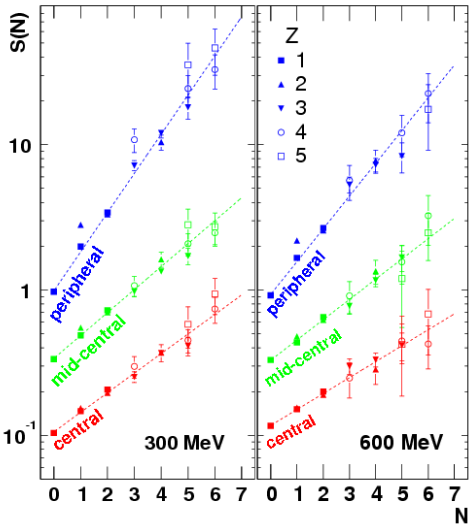

Fig. 15. Scaled isotopic ratios for $^{12}C+^{112,124}Sn$ at 300 (left) and 600 (right) MeV/A. Three different centrality bins are considered.

is observed to decrease with increasing centrality of the reaction and the beam energy (see Fig.15). At the same time, it is observed that the temperature (measured from isotope ratios) of the system increases as a function of the centrality.

4.4 A critique on the extraction of symmetry energy from isoscaling analysis

Eq.(3) suggests that it is possible to extract information on the symmetry energy coefficient from the isoscaling analysis of the data. In the past couple years, there have been many attempts to use Eq.(3) to extract the symmetry energy [39,44,49,19,55]. Nearly all of these efforts assume that the isoscaling parameters obtained from the yield ratios of ground state fragments can be directly compared to the predicted isoscaling parameters obtained from primary fragments produced in statistical or dynamical models. Moreover the quantity $\Delta(Z/A)^2$ and the temperature are obtained from other assumptions which often contradict or are inconsistent with the extraction of the isoscaling parameter $\alpha's$.

To examine this issue further, we investigate the three quantities in Eq.(3), α, $\Delta(Z/A)^2$ and ξ. In ref.[18], AMD simulations for the collisions of the Ca isotopes had been performed. The results of these simulations are shown in Fig.(16) [56]. $^{40}Ca+^{40}$Ca is chosen as system 1.

We note that while α (bottom panel), $\Delta(Z/A)^2$ (middle panel) depend on the reaction systems and the interacting potentials, $\xi = \alpha/(4\Delta(Z/A)^2)$ only depends on the interacting potentials (Gogny (open squares) and Gogny-AS (closed diamonds)). Indeed, as discussed in conjunction with Eq.(8), the linear relation between the isoscaling parameter α and the difference $\Delta(Z/A)^2$) is a general property. These quantities are obtained from the hot fragments produced in the AMD simulations. Assuming that chemical equilibrium is reached, Eq.(3) is fulfilled, i.e. $\xi = E_{sym}(\rho)/T$, and, if the temperature can be estimated, the symmetry energy value can be finally extracted. As expected from isoscaling, α is nearly independent of the charge number of the isotopes.

The primary fragments are then allowed to decay and the corresponding quantities are plotted in Fig.17. Isoscaling is still preserved but the alpha values no longer show a difference between the two interactions. Furthermore, all the three quantities, α, $\Delta(Z/A)^2$ and ξ have different values before and after sequential decays. To extract the correct symmetry energy, ξ, before decay, one must use the values of α and $\Delta(Z/A)^2$ from the primary fragments. All current methods of extracting symmetry energy involves measuring $\alpha's$ using experimental data rather than deducing the values from the primary fragments. Dynamical models have shown that α from the excited primary fragments could be different from α values extracted from final fragments after decay [36,52]. In some cases, the authors use the $\Delta(Z/A)^2$ values interpolated from the AMD simulations using the Ca+Ca systems [57]. This procedure is not justified [52]. Furthermore, this corresponds to using the alpha values from the bottom panel of Figure17 and the $\Delta(Z/A)^2$ values from the middle of Fig.16. Obviously, the method is incorrect. Other authors use the $\Delta(Z/A)^2$ values of the initial compound systems [49]. For our specific example, this corresponds to $\Delta(Z/A)^2$ of 0.0764 and 0.139 for the systems $^{48}Ca+^{48}Ca$ and $^{60}Ca+^{60}Ca$. By convention, $^{40}Ca+^{40}Ca$ is taken as the reference system. Again the method will not yield the correct symmetry energy of the primary fragments.

Some procedure used in extracting the symmetry energy involves a hybrid model which incorporates a dynamical model (such as BUU or AMD) to generate the primary fragments or residues and then use a statistical multifragmentation model to allow the residues to decay to hot fragments [19,54,58]. It should be noticed that in any of the hybrid study, the symmetry energy is not treated in the same way in the two steps. Indeed, if a density dependent symmetry term is used in the evaluation of the

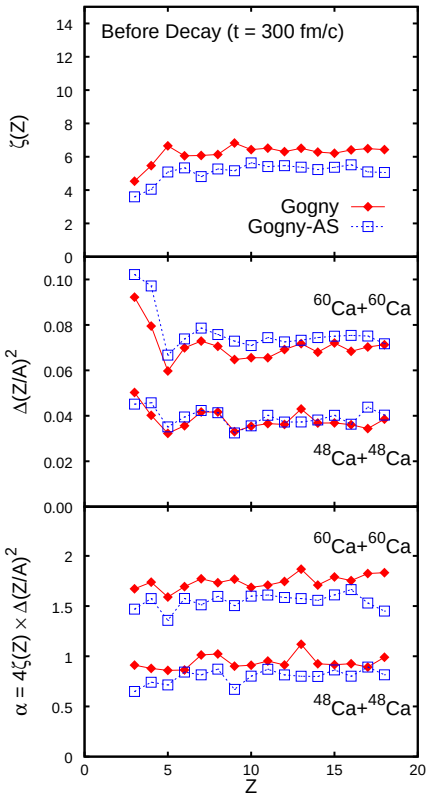

Fig. 16. The three quantities $\xi(Z)$ (top),$\Delta(Z/A)^2$ (middle) and α (bottom) for the primary fragments, as obtained in AMD calculations. The results with the Gogny and Gogny-AS forces are shown by filled diamonds and the open squares, respectively.

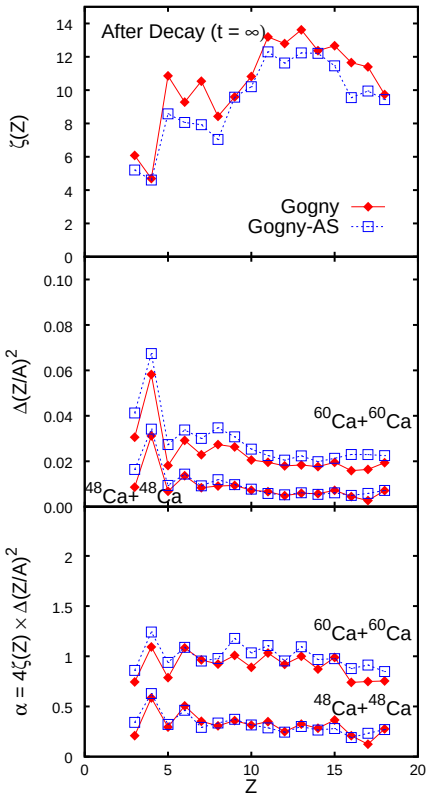

Fig. 17. The same as Fig.(16) but for the final fragments.

pre-equilibrium emission, the same density dependence is not used in the SMM model. Even though in some studies, [49], the density dependence is partly taken into account by changing the symmetry energy constants used in the mass formula in SMM, the lack of temporal evolution and the differences in the effect of sequential decays in the two models are of grave concerns.

Thus isoscaling remains a nice algorithm in data analysis. Unfortunately, it has been elusive to extract symmetry energy using Eq.(3). To make progress in this area, one should include the same density dependence of the symmetry term in the equation of state from start to finish.

5 Isospin transport

In peripheral collisions it is possible to identify projectile-like and target-like residues in model calculations, as well as in experiments. Calculations suggest that at incident energy above 30 MeV per nucleon and for charge - asymmetric reactions, the symmetry term of the nuclear EOS provides a significant driving force that speeds up the isospin equilibration between the two reaction partners. Thus peripheral collisions may allow one to measure the time scales for charge and mass transport and diffusion during the collision. The degree of equilibration, correlated to the interaction time, should provide some insights into transport properties of fermionic systems, in particular give information on transport coefficients of asymmetric nuclear matter [59].

5.1 Insight into isospin transport in nuclear reactions

In asymmetric systems, isospin transport can arise from isospin gradients (diffusion) and from density gradients (drift). Through the low density neck region, density gradients may be present also in binary system. The neutron-excess is pushed towards the low-density regions, because this situation is energetically more favorable. This mechanism can induce isospin transport even in reactions between nuclei with the same N/Z [60].

The role of the EOS in isospin transport mechanisms can be made more explicit by studying the response of nuclear matter, in the presence of neutron and proton density gradients. Since we are mostly facing situations where local thermal equilibrium is reached, we will discuss results obtained within the hydrodynamic limit, where the derivation of the isospin transport coefficients is more transparent.

In such a framework the proton and neutron migration is dictated by the spatial gradients of the corresponding chemical potentials $\mu_{p/n}(\rho_p, \rho_n, T)$, where ρ_p and ρ_n are proton and neutron density and T denotes the tempera-

ture [61,27]. The currents of the two species can be expressed, in terms of the total density $\rho = \rho_n + \rho_p$ and asymmetry $I = (\rho_n - \rho_p)/\rho$, as follows

$$j_n = D_n^\rho \nabla\rho - D_n^I \nabla I \quad (9)$$

$$j_p = D_p^\rho \nabla\rho - D_p^I \nabla I, \quad (10)$$

where D_q^ρ and D_q^I are drift and diffusion coefficients due to density and isospin gradients, respectively:

$$D_q^\rho = ct \left(\frac{\partial \mu_q}{\partial \rho}\right)_{I,T} \quad (11)$$

$$D_q^I = -ct \left(\frac{\partial \mu_q}{\partial I}\right)_{\rho,T}, \qquad (q = n, p) \quad (12)$$

(ct is a negative constant).

They can be expressed as:

$$D_q^\rho = ct[N^{-1} + \frac{\partial U}{\partial \rho} \pm 2I\frac{\partial E_{sym}}{\partial \rho} + O(I^2)] \quad (13)$$

$$D_q^I = \pm 2ct\ \rho[E_{sym} \pm I(\rho\frac{\partial E_{sym}}{\partial \rho} - E_{sym})] \quad (14)$$

$$(+n, -p),$$

where N^{-1} is the level density of symmetric matter at the same density and temperature and $U(\rho)$ is the isoscalar part of the mean-field potential.

One can see that the isovector part of the nuclear interaction enters the coefficients D_q^ρ through the derivative of the total symmetry energy E_{sym}. On the other hand the isospin diffusion coefficients D_q^I depend, in leading order, on the value of the symmetry energy coefficient E_{sym}. Moreover, it appears that the difference of neutron and proton drift coefficients, $D_n^\rho - D_p^\rho = \frac{\partial(\mu_n - \mu_p)}{\partial \rho}$, is equal to $4I\frac{\partial E_{sym}}{\partial \rho}$, as one can simply derive also from the relation $\mu_n - \mu_p = 4E_{sym}I$.

In conclusion, the diffusion appears essentially related to the value of the symmetry energy, while the drift is connected to its derivative. From this study one can see more clearly that the isospin distillation effect, as discussed in Section 3, which originates from the presence of density gradients in the fragmentation process, is sensitive essentially to the derivative of the symmetry energy at low density.

5.2 Experimental studies and comparison with calculations

Experimentally, one examines the isoscaling properties of the fragments originated from the (projectile) residues. Figure 18 shows the isoscaling phenomenon observed in the reaction of ^{124}Sn (projectile) + ^{112}Sn (target) and its inverse reaction ^{112}Sn (projectile) + ^{124}Sn (target) [15]. Unlike the central collision isoscaling data, the slope is larger for the reaction with neutron-rich projectile than the reaction with the proton-rich projectile. Differences

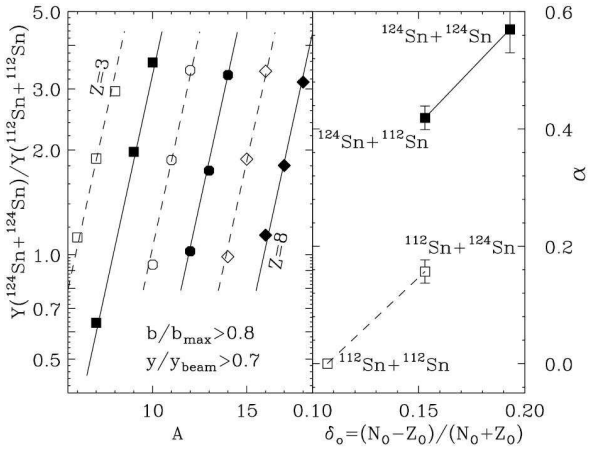

Fig. 18. Isotope yield ratios, as a function of the mass A, for fragments emitted from PLF in peripheral collisions (left). The isoscaling parameters, as obtained in different projectile-target combinations, are compared in the right part of the figure.

in the asymmetric systems reflect the driving force that causes isospin diffusion. As shown before, the force arises from the symmetry term in the equation of state. If the force is weak, one would not expect any isospin mixing to occur and the α value should resemble those of the projectiles in the symmetric systems. In order to quantify the transition from no isospin diffusion to complete mixing, the isospin transport ratio, R_i is used:

$$R_i = \frac{2O_{PT} - O_{PP} - O_{TT}}{O_{PP} - O_{TT}} \quad (15)$$

Here $P, (T)$ stands for the projectile-like (target-like) fragment. The quantities O_i refer, in general, to any isospin dependent quantity, characterizing the fragments at separation time, for the mixed reaction ($PT, 124{+}112$ or $112{+}124$), the reactions between neutron rich ($PP, 124 + 124$), and between neutron poor nuclei ($TT, 112 + 112$), respectively. Similar ratios constructed using free protons have been used as isospin tracer in central heavy ion collisions [62], to check stopping and thermal equilibration. The insensitivity to systematic errors and the ability to calibrate the observables from the two symmetric systems, ^{124}Sn + ^{124}Sn and ^{112}Sn + ^{112}Sn to +1 and -1 offer many advantages. It has been shown that non-isospin effects such as effects from Coulomb force will be largely cancelled using the isospin transport ratio. Furthermore, in comparisons with calculations that cannot predict the same experimental observables, due to model limitations, one can use another observable to construct the isospin transport ratios as long as both the experimental and theoretical observables are linearly related to each other. For example, in model calculations, one can use the asymmetry $I = (N - Z)/A$ of the emitting source, instead of isoscaling, to evaluate the transport (imbalance) ratio since, to the first order, α and I are linearly related. In fact, as we have seen previously, α, as extracted from primary fragments, is related to the difference $(\frac{Z_1^2}{A_1^2} - \frac{Z_2^2}{A_2^2})$, which for not too large asymmetries can be rewritten as $(I_2 - I_1)/2$.

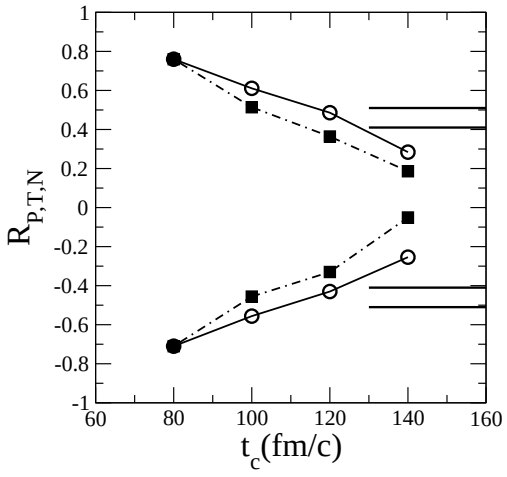

Fig. 19. *The isospin transport ratio $R_{P,T}$, Eq.(15), for the asy-"soft" (full squares) and asysuperstiff (circles) EOS's as a function of the interaction time t_c, corresponding to different impact parameter b, in the range 6-10 fm. The band between the two solid lines corresponds to the experimental data of [15]. The triangles represent the imbalance ratio calculated for the neck fragments, in ternary events.*

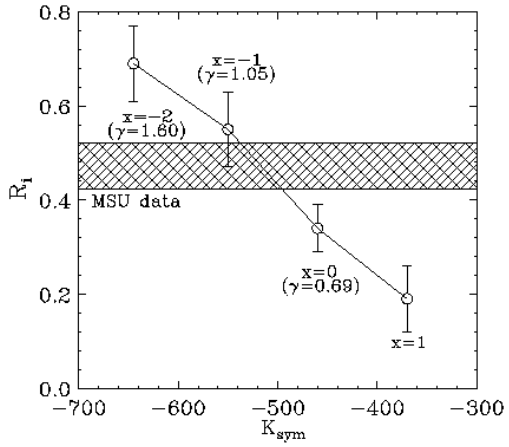

Fig. 20. Imbalance ratio, relative to peripheral collisions of ^{124}Sn + ^{112}Sn, E/A = 50 MeV, as obtained in the data (shaded area) and in model calculations using different parameterizations of the symmetry energy.

The linear relation between α and I has been confirmed also experimentally [29], suggesting that it holds also for the isoscaling parameters extracted from the final fragments. Hence, the asymmetry of projectile-like or target-like residues can be used as the observable O in Eq.(15).

The dependence of isospin transport (and equilibration) on the centrality of the reaction has been investigated in Ref.[63] using SMF simulations without momentum dependence. Fig.19 shows the imbalance ratio as a function of the interaction time t_c among the two reaction partners, that is inversely related to the impact parameter, for two asy-EOS's: a very "stiff" and a "soft" (SKM*) interactions. A more detailed analysis shows that it is possible to explicitly estimate the effect of isospin transport and pre-equilibrium emission on the transport ratios R. The interplay between the two processes leads to a stronger equilibration for asy-"soft" EOS, as it is evidenced by the isospin transport (imbalance) ratio. Actually, in the asy-"stiff" case, a larger isospin transfer is observed in the calculations, due to the presence of density gradients, directed from PLF and TLF towards the neck region, in line with the analyical predictions illustrated above. Indeed, in the asy-"stiff" case, the derivative of the symmetry energy, just below normal density, acquires larger values. However, we observe a kind of compensation between the asymmetry of the matter transferred from projectile to target (I_{PT}) and from target to projectile(I_{TP}), so finally isospin equilibration is more effective in the asy-"soft" case.

In ref.[15,64] BUU calculations which use different density dependence of the symmetry terms in the equation of state are performed for the same system at b=6 fm.

In Fig.20, the parameter term x indicates the stiffness of the symmetry term, ranging from a "soft" behaviour (larger x) to a "stiff" behaviour (negative x.) Momentum dependence is included in the calculations. Within error bars, the isospin transport ratio R_i exhibits a decreasing behaviour with the softness of the symmetry term suggesting that the driving force for isospin equilibration is much larger for the "soft" interaction. Using the neutron isoscaling fitting parameter α as the experimental isospin observable O in Eq.(15), the isospin transport ratios of the two asymmetric systems shown in the right panel of Fig.18 appear as the two horizontal lines in Figures19,20. So, assuming that data can be directly compared with calculations performed at b=6 fm, a better agreement is obtained when using a "stiff" asymmetry term, in the range $x = -2, -1$. Without including momentum dependence in the calculations, a stiffer symmetry term would be needed to fit the data (see Fig.19 at 140 fm/c). This is due to the fact that the overall dynamics becomes more repulsive when the momentum dependence is included and isospin equilibration depends not only on the strength of the symmetry term, but also on the system interacting time.

It should be noticed that this comparison is well suited only if one assumes that PLF and TLF fragments are at around normal density, independent of the parameterization adopted for the symmetry energy. Otherwise the isoscaling parameter cannot be simply related only to the N/Z of the source, but would also depend on the value of the symmetry energy, that is model dependent. It would be interesting to check this hypothesis using a model that includes fragmentation (such as AMD), and calculating the imbalance ratio directly from the isotope yields, as it is done in the experiments. In this way one would better test the sensitivity of the results to the behaviour of the symmetry energy. In other words, as discussed in Section 4.4, it is essential to consider the density dependence of the symmetry energy also in the fragmentation process.

The dependence of the N/Z versus the excitation energy of the system has been studied for the INDRA reactions, Ni+Ni and Ni+Au at 52 and 74 MeV/A [65],

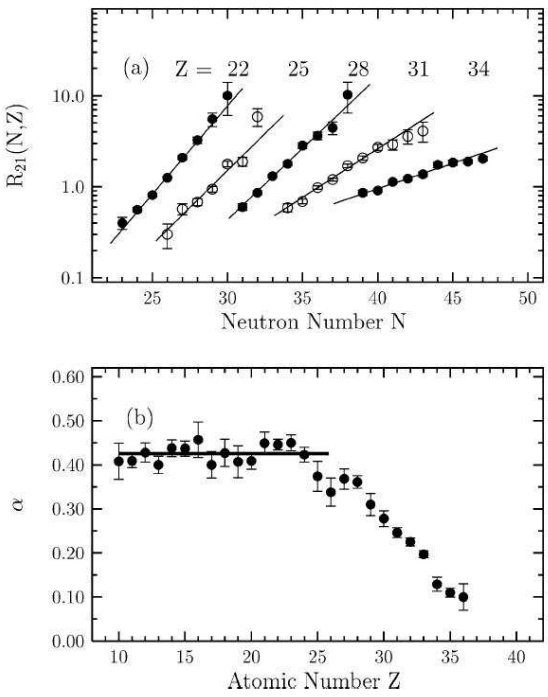

Fig. 21. a) Yield ratios $R_{21}(N,Z)$ of projectile residues from the reactions $^{86}Kr + ^{112,124}Sn$ at 25 MeV/A, with respect to N, for the Z's indicated. b) Isoscaling parameter α versus the charge of the fragment Z. The straight line is a constant value fit for the lighter fragments Z = 10-26.

looking at the reconstructed PLF, in binary collisions. In the symmetric case, N/Z is seen to increase with centrality due to a proton-rich pre-equilibrium emission. For the Ni+Au case, it is possible to observe isospin equilibration among the reaction partners.

Also for the analysis presented in Ref.[55], the goal was to extract the N/Z of the PLF sources and hence to discuss isospin equilibration between projectile and target. The systems $^{86}kr + ^{112,124}Sn$ at 25 MeV/A have been considered. The isoscaling parameter α, as a function of the charge Z of projectile residue, exhibits a plateau, that indicate that these fragments come from sources with "equilibrated" N/Z. Then a decrease of α is observed, as Z increases, that should correspond to fragments coming from PLF's formed in more peripheral reactions, hence more similar in the two systems considered.

5.3 Conclusions and outlook

From the results discussed above, one can conclude that several indications on the density behaviour of the symmetry potential can be extracted from the study of reactions with charge asymmetric systems in the Fermi energy domain. The isotopic content of emitted light particles and IMF's, as well as the reconstructed degree of N/Z equilibration between reaction partners, bear important information on the symmetry energy behaviour. We summarize below the main conclusions, as well as improvements and new studies that can be envisaged.

– In model calculations, the isotopic content of pre - equilibrium emission appears quite sensitive to the stiffness of the symmetry term, even to its momentum dependence. A more neutron-rich pre-equilibrium emission is expected for higher values of the symmetry energy. In fragment formation the degree of isospin fractionation (i.e. the transfer of the neutron excess towards the gaseous phase) is sensitive to the slope of the symmetry energy at low density. From the comparison with experimental data, some indication has emerged about a "stiff" behaviour of the symmetry energy.

– The isoscaling analysis, based on the comparison of the isotopic content of fragments emitted from systems with different initial asymmetries, allows to put in better evidence isospin effects and, in situations where equilibrium is reached, could in principle be used to extract the value of the symmetry energy in the conditions of density and temperature where fragmentation happens. However, it is not so easy to disentangle between the predictions given by the different parameterizations. Indeed not only the isoscaling parameters reflect the width of the isotopic distributions, but they are quite sensitive to the difference $\Delta(Z/A)^2$ between the fragments asymmetries of the two compared systems, that is also largely influenced by the symmetry energy behaviour. Hence compensation effects may diminish the sensitivity of the final results to the asy-EOS. Moreover, as shown by dynamical simulations, large secondary decays may reduce significantly the differences coming from different symmetry terms in the EOS used in the models.

It would be important to perform a cross-check of model predictions against several experimental observables, sensitive to the different phases of a reaction, from pre - equilibrium emission to fragmentation and de - excitation stage. This allows better identification of the isotopic content of the gas and liquid phases, that is essential for the analysis of the de-excitation process of the excited primary products and related observables (such as isoscaling). The use of models that can follow the whole path of the reaction is highly desirable. This would also allow to ascertain the fragmentation mechanism and the way the system approaches chemical freeze-out. The study of correlations between fragment isotopic content and kinematical properties can be envisaged as a tool to learn about time scales for fragment formation and N/Z equilibration.

– In semi-peripheral collisions, it is interesting to compare the behaviour of reactions with different entrance channel asymmetries to investigate isospin exchange between projectile and target. Indeed the N/Z equilibration among the reaction partners gives information about the strength of the symmetry term. However, it should be noticed that the amount of isospin exchange is also strictly connected to the interaction time, along which the two reaction partners are in contact. This is clearly influenced also by the isoscalar part of the nuclear interaction. Hence the sensitivity of this observable to the value of the symmetry energy is not so transparent.

The study of the interplay between isoscalar and isovector parts of the nuclear interaction in the reaction dynamics deserves further attention.

References

1. "It is important to put the properties of *neutron* matter at *subnuclear* densities on as firm a footing as possible, not only for astrophysical applications, but also for interpreting terrestrial experiments with coming radioactive beam facilities" C.J. Pethick and D.G. Ravenhall, in ref.[8].
2. I. Bombaci, T.T.S. Kuo and U. Lombardo, Phys. Reports.**242** (1994) 165 .
   I. Bombaci, Phys. Rev. C55, (1997) 1
3. M.Prakash et al., Phys.Rep.**280**, (1997) 1
4. I.M.Irvine, *Neutron Stars* (Oxford Univ. Press 1978)
5. J.M.Lattimer et al., Phys.Rev.Lett.**66**, (1991) 2701
6. D.Pines, R.Tamagaki and S.Tsuruta, *Neutron Stars* (Addison-Wesley N.Y. 1992)
7. K.Sumiyashi and H.Toki, Astro.Phys.Jour.**422**, (1994) 700
8. C.J.Pethick and D.G.Ravenhall, *The Lives of Neutron Stars* NATO ASI Series C **450**, (1995) 59-70
9. C.H.Lee, Phys.Rep.**275**, (1996) 255
10. H.Mueller and B.D.Serot, Phys.Rev.**C52**, (1995) 2072
11. Bao-An Li and C.M.Ko, Nucl.Phys.**A618**, (1997) 498
12. M.Colonna, M.Di Toro and A.Larionov, Phys.Lett.**B428**, (1998) 1
13. V.Baran, M. Colonna, M. DiToro and V.Greco, Phys.Rev.Lett.**86**, (2001) 4492
14. M.Colonna, Ph.Chomaz and S.Ayik, Phys. Rev. Lett. **88**, (2002) 122701
15. M.B.Tsang, T.X.Liu, L.Shi et al., Phys. Rev. Lett.**92**, (2004) 062701
16. J.Y.Liu, W.J.Guo, Y.Z.Xing et al., Phys. Rev.**C70**, (2004) 034610
17. J.Y.Liu, W.J.Guo, Y.Z.Xing et al., Nucl. Phys.**A726**, (2003) 123
18. A.Ono, P.Danielewicz, W.A.Friedman et al., Phys. Rev. C **68**, (2003) 051601(R).
19. W.P.Tan, B-A Li, R.Donangelo, et al., Phys. Rev.**C64**, (2001) 051901
20. B-A Li, C.M.Ko, Z.Z.Ren, Phys. Rev. Lett.**78**, (1997) 1644
21. V. Baran *et al.*, Nucl. Phys. **A 703**, (2002) 603-632.
22. P.Sapienza et al., Phys. Rev. Lett. **87** (2001) 070701, and ref.s therein
23. B-A Li, C.B.Das, S.Das Gupta et al., Nucl. Phys.**A735**, (2004) 563
24. J.Rizzo et al., Nucl.Phys.**A732**, (2004) 202-217
25. J.Y. Liu, W.J.Guo, Y.Z.Xing et al., High Energy Phys. Nuc.**29**, (2005) 456
26. J.Rizzo, M.Colonna and M. di Toro, arXiv: nucl-th/0508008.
27. V. Baran, M. Colonna, V. Greco, M. DiToro, Phys.Rep. **410**, (2005) 235
28. J.Margueron and Ph.Chomaz, Phys. Rev. **C67**, (2003) 041602
29. H.S. Xu et al., Phys. Rev. Lett. **85**, (2000) 716
30. M.B. Tsang, W.A.Friedman, C.K.Gelbke et al., Phys. Rev. Lett.**86**, (2001) 5023
31. M.Veselsky, R.W.Ibbotson, R.Laforest et al., Phys. Rev.**C62**, (2000) 041605
32. W.P. Tan, S.R.Souza, R.J.Charity et al., Phys. Rev.**C68**, (2003) 034609
33. Kunde et al., Phys. Rev. Lett. **77**, (1996) 2897.
34. M.L. Miller et al., Phys Rev. Lett. **82**, (1999) 1399
35. Ph.Chomaz and F.Gulminelli, Phys. Lett. **B447**, (1999) 221
36. T.X.Liu, M.J. van Goethem, X.D.Liu et al., Phys. Rev.**C69**, (2004) 014603
37. C. Sfienti, P.Adrich, T.Aumann et al., Nucl. Phys.**A749** , (2005) 83C
38. P.Milazzo et al., Phys. Rev. **C62**, (2000) 041602
39. D.V. Shetty, S.J.Yennello, E.Martin et al., Phys. Rev.**C68** , (2003) 021602
40. G.A.Souliotis, M.Veselsky, D.V.Shetty et al., Nucl. Phys.**A746** , (2004) 526C
41. M.N. Andronenko, L.N.Andronenko, W.Neubert, Prog. Theor. Phys. Supp.**146**, (2002) 538
42. M. Veselsky, G.A.Souliotis, M.Jandel, Phys. Rev.**C69**, (2004) 044607
43. W.A. Friedman, Phys. Rev. **C69**, (2004) 031601
44. A.S. Botvina, O.V. Lozhkin and W. Trautmann, Phys. Rev. **C65**, (2002) 044610
45. W.A. Friedman, Phys. Rev. **C42**, (1990) 667
46. M.B.Tsang et al., Phys. Rev. **C64**, (2001) 054615
47. A.D.Raduta, Eur.Phys.J.**A24**, (2005) 85
48. Y.G. Ma et al., Phys. Rev. **C69**, (2004) 064610
49. A. Le Fevre, G.Auger, M.L.Begemann-Blaich et al., Phys. Rev. Lett.**94**, (2005) 162701
50. C.O. Dorso et al., arXiv:nucl-th/0504036
51. M. Colonna and F. Matera, Phys. Rev. **C71**, (2005) 064605.
52. A.Ono et al., arXiv:nucl-ex/0507018
53. M.Colonna et al., Phys. Rev. **C47**, (1993) 1395.
54. D.V. Shetty, A.S.Botvina, S.J.Yennello et al., Phys. Rev.**C71**, (2005) 024602;
    D.V.Shetty, A.S.Botvina, S.J.Yennello et al., Phys. Rev.**C71**, (2005) 029903(E)
55. G.A. Souliotis, M.Veselsky, D.Shetty et al., Phys. Lett.**B588**, (2004) 35;
    G.A.Souliotis, D.V.Shetty, M.Veselsky et al., Phys. Rev.**C68**, (2003) 024605
56. A.Ono et al., Proceedings for VI Latin American Symposium on Nuclear Physics and Applications, Iguazu, Argentina (2005), to be published in Acta Phys. Hung. A.
57. D.V. Shetty, S.J.Yennello, A.S.Botvina et al., Phys. Rev.**C70** , (2004) 011601
58. E.Geraci et al., Nucl. Phys.**A732**, (2004) 173-201.
59. L. Shi and P. Danielewicz, Phys.Rev. **C68**, (2003) 064604.
60. R.Lionti, V.Baran, M.Colonna and M.Di Toro, Phys. Lett. **B625**, (2005) 33
61. R. Balian, *From Microphysics to Macrophysics*, vol II, (Springer Verlag, Berlin 1992)
62. F.Rami et al., Phys.Rev.Lett. **84**, (2000) 1120
63. V.Baran, M.Colonna, M.Di Toro et al., arXiv: nucl-th/0506078, Phys. Rev. C in press
64. L-W Chen, C-M Ko, B-A Li, Phys. Rev. Lett.**94**, (2005) 032701
65. E. Galichet et al., submitted to Nucl.Phys.A